Second International Symposium on Marine Propulsors
smp'11, Hamburg, Germany, June 2011

Propeller Optimisation Considering Sheet Cavitation and Hull Interaction

FlorianVesting[1], Rickard Bensow[1]

[1]Department of Shipping and Marine Technology, Chalmers University of Technology, Gothenburg, Sweden

ABSTRACT

This paper presents an optimisation of a propeller blade with the propeller operating in behind conditions and considering sheet cavitation. A genetic optimisation algorithm is used with multiple objectives considered: The efficiency is maximized while the propeller induced pressure pulses are minimised. The blade design is constrained surveying cavity occurrence predicted from a vortex lattice method. In this investigation, the effect of the propeller on the flow field around the stern of the ship is taken into account by an iterative update of the effective wake, computed using a zonal approach for the hull flow simulation. The chosen optimal propeller display reduced pressure pulses and cavitation extent while maintaining the efficiency of the original design.

Keywords

Genetic optimisation, propeller-hull interaction, RANS, vortex lattice method, cavitation prediction

1 INTRODUCTION

The flow field behind a ship in motion is disturbed by pressure and velocity fluctuations induced from the hull. Consequently, a propeller working behind the ship experiences a highly inhomogeneous inflow. This causes a varying load on the propeller blade during one revolution, resulting in a local pressure drop around the blade. Depending on the operation conditions, e.g., submergence of the propeller shaft or rotational speed, the pressure sags below vapour pressure and cavitation, i.e., vapour pockets in the liquid, can be observed at the propeller. When again entering high pressure regions, the cavities collapse extremely rapidly and may cause noise and vibration, transferred to the ship's hull, and causing erosion on the propeller or the rudder.

This is a major concern in the propeller design and a common philosophy has been to avoid cavitation within the range of operating condition. Nevertheless, the demand for high-performance propellers makes this no longer feasible, and the presence of cavitation needs to be accepted and considered in design, while comfort levels, with respect to noise and vibrations need to be maintained or even improved as well. Furthermore, a typical procedure is to design a propeller in a given wake, which was measured behind the ship during towing tank experiments; the corresponding action of the propeller on the flow field is then neglected. These interaction effects have an impact on both the total propulsive efficiency as well as on the cavitation behaviour. This means that the design procedure loses a potential benefit from propulsor-hull interaction, and at the same time, can give an erroneous cavitation prediction. Both of these effects are considered in the automated design process described in this paper.

The present work follows an investigation of Han et al (2006a), where a cavitating propeller was optimised in a given wake, with the objective to maximise the efficiency and minimise the propeller induced pressure fluctuations by tuning the propeller blade geometry. In addition, a near-optimum propeller and an off-design propeller were optimised behind a ship at full scale by minimising the delivered power for a certain speed (Han et al 2006b), but not considering cavitation. Lee et al (2006) presented different methods to analyse the propeller-induced pressure pulses and their effect on hull vibrations, utilising computational fluid dynamics (CFD) for the prediction of pressure fluctuations and finite element methods (FEM) to compute their impact on the ship structure, as state-of-the-art analysis at American Bureau of Shipping (ABS). It was concluded that the propeller-induced pressure phase differences have an important influence on structure vibration. Thus, as a logical continuation of previous work, the aim of this work is to study the automated optimisation of the propeller geometry considering cavitation in conditions behind a ship.

The computations are carried out in full scale for a reefer with Lpp around 170m that operates at high speed (Fn = 0.27) and, hence, operates with a highly loaded propeller; Figure 1 depicts the lines plan of the ship geometry. Since the rudder should be seen as a part of the propulsor (Kuiper 2010), it is also included in the model.

The computational approach used to assess this engineering task is to compute the hull flow with a viscous RANS methodology, using SHIPFLOW, coupled to an inviscid potential formulation for the propeller in MPUF-3A. The geometry variation as well as the constraints-, parameter-, and objectives-management are

controlled by the FRIENDSHIP-SYSTEMS Framework. The optimisation is carried out with the built-in multi-objective evolutionary algorithm NSGA-II.

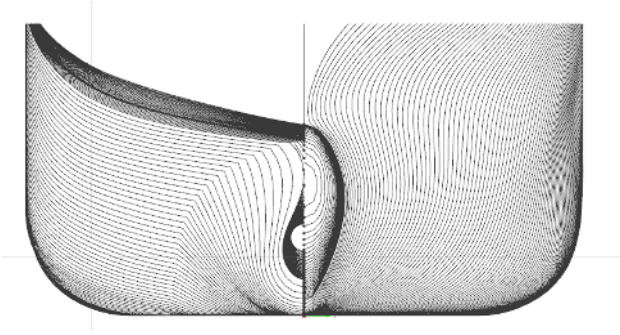

Figure 1: Lines Plan of the Investigated Ship

Table 1: Ship Data

Type of ship		reefer ship
Length between PP	[m]	174.53
Beam, waterline	[m]	25.14
Draught, waterline	[m]	8.5
Propeller diameter D	[m]	6.3
C_B	[-]	0.62
Blade tip clearance	[%]	23.8 of propeller D
Number of blades	[-]	5

2 NUMERICAL METHODS

The computations were performed by using the CFD software suit SHIPFLOW 4.4 for investigating the flow, the corresponding forces, and the propulsion characteristics of a ship design. The approach used in this work is based on a zonal approach using three types of methods to predict the flow around the hull through a division of the domain into three zones: i) A potential-flow solver is applied to solve the inviscid flow around the hull and compute the free-surface in Zone 1; ii) a momentum integral method is used for the prediction of the viscous flow in the thin boundary layer on the forward half of the ship in Zone 2; and iii) in Zone 3, the viscous wake flow is solved using RANS.

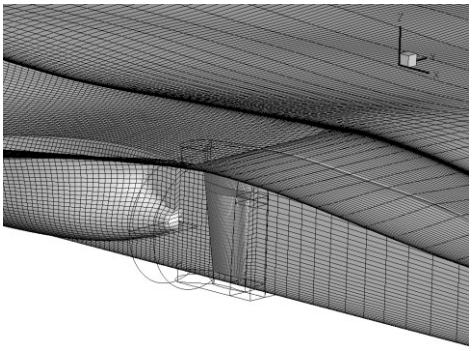

Figure 2: Overlapping Volume Grids at the Aft Part of the Ship with Prescribed Free Surface

Sub grids for a rudder and the propeller are introduced through overlapping grids, see Figure 2. Since the working propeller will have an asymmetrical effect on the flow, no symmetry plane was considered. The water plane can be treated either as a double model or with a prescribed free surface solution, obtained from potential flow method; no viscous free surface approach is yet available in SHIPFLOW. The solver for steady incompressible flow is based on a Roe scheme for discretization of the convective terms, for more details see Regnström (2007).

To perform the study for a propelled ship, the RANS solver included in SHIPFLOW (XCHAP) is combined with a vortex-lattice method, VLM, (MPUF-3A of University of Texas) for the analysis of the unsteady cavitating flow; see Kinnas (1985) and Kerwin et al (1986) for more details on the propeller code. To adapt the effective wake and obtain the body forces, computed by MPUF-3A, the propeller induced velocity are subtracted from the total wake (by the code UTCFDIF). The VLM calculates the force distribution of each propeller blade position and UTCFDIF interpolates the forces on the embedded propeller grid. The force field is read in by SHIPFLOW and added as a volume force on the right hand side of the equation. The update is performed every 10th iteration of the RANS solver. Thus, the fluid passing the propeller plane experiences an acceleration corresponding to the propeller action. This iterative procedure is sketched in Figure 3.

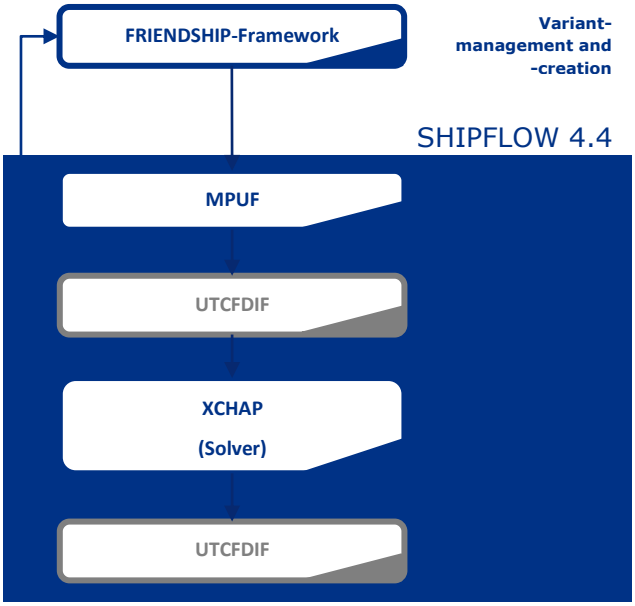

Figure 3: Iterative Update Procedure Determine the Effective Wake within the Optimisation Procedure

The hydrodynamic pressure pulses due to the blade passing beneath the hull and dynamic cavitation on the blade due to non-uniform inflow are rated utilising puf3fpp, which is a simplified version of HULFPP program developed by Sun et al (2007). It computes the first, second and third pressure amplitude harmonics from the propeller dynamics (including sheet cavitation) on the

velocity potential of the sources solved by MPUF-3A. The influence of the hull surface is introduced with the concept of solid boundary factors (SBF). Thus, the pressure acting on the hull is increased significantly compared to the free field pressure. Carlton (2007) suggests setting this empirical factor to a value of 1.8 in ship calculations. However, in this investigation we use 1.9 according to Han (2006a). An increase is equivalent to conservative view, since flat plates with infinitive stiffness obtain a SBF of 2.0.

2.1 Flow solver configuration

In the present work, all computations were carried out applying EASM turbulence model (Regnström 2007). The grids were constructed with y^+ = 0.7; thus, no wall functions need to be introduced. According to Zou et al (2010), this turbulence model produced the most accurate wake flow. The grid for the global approach has 6.63 million cells, while for the zonal approach about half, 3.42 million cells, is considered sufficient. This is based on the validation exercise presented by Han et al (2006b). In order to make certain that the zonal approach in SHIPFLOW 4.4 gives the appropriate results and can be used in the optimisation, which strongly benefit from the smaller grid size, an exercise comparing the global and zonal approaches has been performed. Moreover, the effect of a double model simulation compared with using prescribed free surface has been tested. These results will only be briefly reviewed here.

Both Han et al (2006b) and Zou et al (2010) have investigated the numerical wake prediction from SHIPFLOW. The conclusion is that the zonal approach is accurate enough to capture most of the flow characteristics with reasonable accuracy. This is also confirmed in our investigations. Furthermore, using a wavy free surface decreases the differences. The conclusion is also independently verified by Visonneau (2010) in his review of local flow analysis for the Gothenburg 2010 workshop.

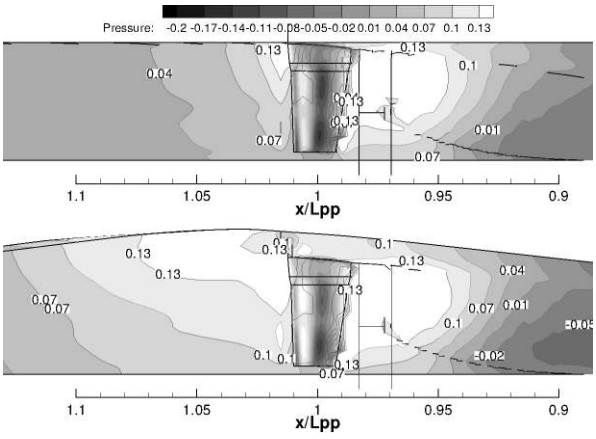

Figure 4: Pressure Distribution around the Aft Part of the Hull for Double Model Solution (above) and Prescribed Free Surface Solution (below)

In Figure 4, we compare results using a double model and a wavy free surface (as computed using potential flow approach) by showing the pressure distribution for the aft part of the hull without a propeller. The upper plot shows the double model solution, the lower one the solution when the free surface is included. From this, one can see the influence of a wave crest on the pressure distribution. This leads to a thrust deduction and, hence, to a higher loaded propeller and cannot be neglected.

Thus, SHIPFLOW is set up with the zonal approach and a prescribed free surface for the optimisation. This yields an advantage regarding computational time, crucial in automated optimisation, while having a reasonable accuracy.

2.2 Analysis of cavitating propellers

The propeller geometry is represented by a lattice of discrete vortex and source elements on the mean camber-surface of the blade. The chord wise distribution follows the half cosine spacing of the singularities. The cavity and the blade thickness are represented by the sources. While the thickness is known from the beginning, the cavity sources have to be solved for each time step. Vortex and cavity source elements are extended downstream forming a transient wake, see Figure 5. The solution of the vortex strength is obtained by solving the tangency flow boundary condition at a set of control points (collocation points); a detailed description can be found in Kinnas (1985). The vortex strengths are computed for the key-blade only, to save computational cost and one assumes the loading on the other blades correspond to that previously found for the key-blade. In Figure 5, the key-blade and its wake is pictured with solid lines. It has a denser discretisation than the other blades.

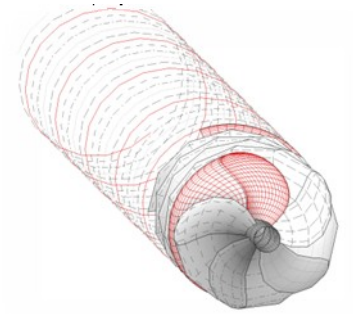

Figure 5: Discretization of the Propeller in VLM

The discretisation of the propeller blade is in accordance with the recommended settings for reasonable accurate and quick results, He et al (2010). The time step size is corresponding to rotation angle for each blade position at which the cavitation is determined. This is set to the maximum possible resolution of 6°. These settings showed a good agreement in a quantitative comparison with experimental results for the sheet cavitation development and dissipation.

3 OPTIMISATION METHOD

The optimisation problem is formulated in the standard form as:

$$min[f_1(\vec{x}), f_2(\vec{x}), \dots, f_k(\vec{x})],$$

where k is the number of objectives and $\vec{x}$ the vector of design variables:

$$\vec{x} = [x_1, x_2, \dots, x_n]^T.$$

The objective functions f_k are in general subject to several equality and inequality constraints as:

$$h_i = 0 \quad i = 1, \dots, I,$$
$$g_j \leq 0 \quad j = 1, \dots, J.$$

The solution of the optimisation problem will be obtained when the design vector satisfy all constraints and the best solution is not worse in any other objective and better at least in one objective, than the other solutions. In other words, there is no other feasible vector $\vec{x}$ that decreases one objective without increasing at least another one. This is a Pareto optimum. However, this concept leads to a set of solutions until the minimum is found. Such trade-off solutions are then called Pareto optimal set (Abraham et al 2005).

The evolutionary algorithm selected, the non-dominated sorting algorithm II (NSGA-II) (Deb et al 2000), is based on several levels of classification according to non-domination. Each solution must be reviewed to find if it is dominated. For more details on the fast-non-dominated-sorting, see Deb et al (2000). The first generation P_0 is created randomly. Before creating the first child generation, the solutions are ranked according to their level of non-domination corresponding with a fitness value. By classified selection, recombination and mutation, the first child generation is produced with respect to the fitness value. Since the individuals in the first rank have the lowest values, they always get the most copies and minimisation of fitness is assumed (Deb et al 2000). For the following offspring, elitism is introduced when comparing the individuals of parent and child generation in a combined population R_t, with the population size 2N.

All individuals of R_t are sorted according to non-domination, as mentioned above. The first rank now contains the best solutions of the combined population and will be emphasised for the new population P_{t+1}. This new population of size N will be filled up with members of the best non-dominated sets successively until no more individual can be accommodated. The individuals of the last non-dominated rank to fill up P_{t+1} are sorted using the crowded operator. The crowded operator introduced by Deb et al (2000), is based on a density of solution estimations by calculating the averaged distance between the solutions in each direction of the objectives. Solutions located in a less crowded region are considered preferred. This allows searching for non-dominated regions and converging to these regions. In addition, NSGA-II is computationally efficient and deals with a population of possible solutions simultaneously which allows finding several members of the Pareto optima instead of handling a series of separate runs. This is especially interesting for the use of parallel computation of the variants.

3.1 Geometry variation procedure

With simulations becoming more and more accurate, an increasing computational power and the appearance of useful tools for creating mathematical complex geometrical representations, computer-aided engineering (CAE) is increasingly used to produce and evaluate shapes automatically. This kind of simulation driven design is more and more used for the design of optimal components in the marine industry (Abt et al 2009). An important precondition with respect to simulation driven design, is that the embedded computer-aided design (CAD) software provides a suitable geometry and a systematic variant creation. The optimisation procedure is tightly coupled with the set of input parameters. Thus, an efficient variant creation with a low number of parameters that always provide a feasible geometry is a key-function to effective automated optimisation.

The (CAE) software FRIENDSHIP-Framework provides fully parametric modelling options, where the geometry is purely described through a set of parameters, as well as partial parametric modelling, where variants are created by changing an existing geometry; the study presented here combines both types of modelling. A set of 2D profiles is imported from the baseline propeller design. Each is in addition defined by a set of arguments, like chord length and camber distribution, which are linked to functional distribution curves depending on the radius of the propeller; thus the profile changes along the radius, following the parameter distribution curve and forming a smooth surface representation. Finally, parameter curves for the skew, thickness pitch and rake complete the blade description.

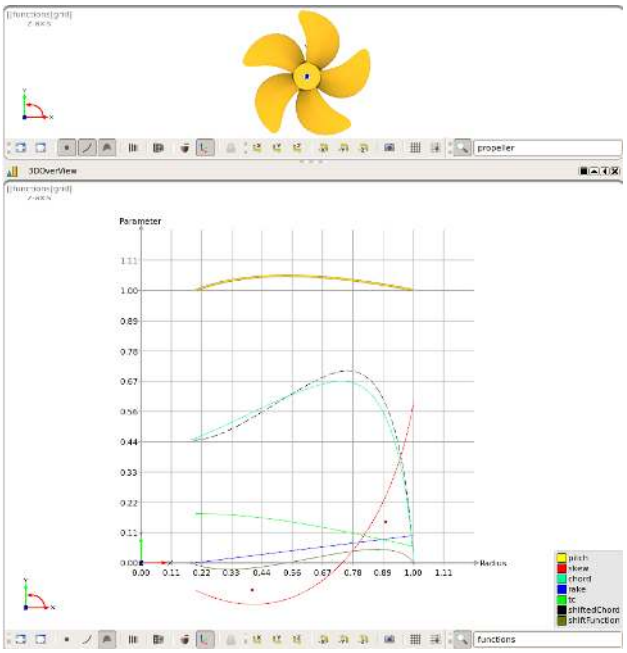

Figure 6: Propeller Blade Describing Parameter Curves with Delta Shift in FRIENDSHIP-Framework

Changes for variant creation are then applied on the imported baseline parameter curves by shifting the given set of original curves; see Figure 6 for an example set of

curves. Here the dashed line represents a shifted parameter curve for the chord length. The delta value of the shift is thereby provided from a B-spline curve (the curve named "shiftFunction" in Figure 6) which is defined by less control points than the original curve but still allows for smooth change of the original parameter. Overall, 12 control points are introduced to modify the given geometry.

The variant geometry for the manipulated propeller-blade is finally translated to a set of sectional profiles according to the MPUF-3A geometry input. The optimisation procedure was carried out utilising the Frameworks generic integration for coupling the modelling and the flow solver.

3.2 Cavitation consideration in objectives and constraints formulation

Cavitation nuisance development is very complex and involves high-grade unsteady flow and dynamic behaviour of cavitation, material properties and structural response. Erosion damage can be caused either from a spherical cavitation bubble which develops an asymmetric shape, due to the proximity to the solid surface, and finally collapses causing a rapidly accelerated micro-jet with the effect of high local pressure amplitude directed towards the solid surface; or from collapsing bubbles, more distant from the surface, that create an intense pressure wave which may induce high stress on the surface. Both processes, of course, also yield noise.

Grekula (2010) describes the latter phenomenon with the concept of focusing energy in time and space during the collapse acceleration. Such focusing cavities are almost always generated from a large-scale cavity and, according to Bark et al (2004); the large-scale cavity is related to the global flow and thus gives a relation between the global flow and the erosion risk.

Detailed discussion of cavitation erosion is out of the scope of this paper, and a reliable consideration of this effect using a VLM code is subject to further research. However, here we outline the line of thought by discussing a shed cavity. This mechanism is strongly dictated from the re-entrant flow, which in turn depends on the shape of the cavity closure line; a convex shape of the closure line appears to be more unstable. Foeth (2008) concluded in an investigation for an isolated sheet cavity on three-dimensional hydrofoils that for any convex cavity closure line, the side-entrant component of the re-entrant flow focuses on the aft region and may cause the local brake-off with shedding cavities.

Certainly a VLM cannot capture the travelling or focusing cavities. However, MPUF-3A and similar codes can nevertheless yield valuable indications at an early design stage since it is possible to predict sheet cavitation extent on a propeller blade. Thus, by constraining the sheet cavity closure line, it may be possible to decrease the risk of re-entrant flow causing shedding, leading to a possibly erosive cavity. So, based on the computed cavitation extent, the cavitation length at various sections of the blade is then constrained in this investigation. Furthermore, also the cavitation thickness can indicate the risk of re-entrant flows, which is here constrained by the sectional cavitation area. As mentioned above, exactly which shapes of the sheet cavitation extent to reject is subject to future research, and the inclusion here is intended as a concept idea. An apparent risk here is that the space of feasible designs is restricted by, once again, not allowing enough cavitation.

Based on the above discussion, it is the task to merge the results available from the propeller performance program with the desired formulation of constraints. Figure 7 shows the cavitation solution for the baseline blade design at 0° position. The sheet cavitation is predicted at certain sections of the blade in chord wise direction, for every position (every sixth degree) of the blade. In this investigation it is assumed that the most dangerous cavitation occurs at the blade position where the maximum cavitation volume is predicted, which is one of the constraints. All following results for the cavitation constraints refer to the blade position with the maximum volume. To control the shape of the cavity closure, mainly to avoid shedding caused by closure lines like B in Figure 7 or indication for developing a tip vortex with thick and long sheet (A in Figure 7), the length of each cavitation section is constrained. A rapidly growing cavity will be avoided either by a certain maximal length or a growing factor regarding the length of the previous section. In addition, the maximal cavitation area appearing on the certain blade with maximum volume is constrained.

Furthermore, the Keller criterion,

$$\left(\frac{A_E}{A_0}\right)_{min} = \left(\frac{A_E}{A_0}\right) - \frac{[(1.3+0.3Z)T]}{[(p_0-p_v)D^2]} + k, \qquad (1)$$

introduced by Han (2006a), is adopted for monitoring the cavitation extent with respect to the performance of the propeller. Here Z is the number of blades, T the generated thrust, and k a user defined coefficient set to 0.05.

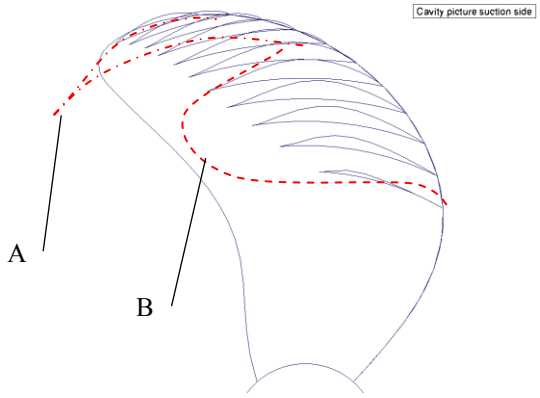

Figure 7: Cavitation Extent and Preventable Cavity Closure (A and B)

The final constraint is an equality constraint on the ship speed. Since self-propulsion is considered, this is a natural constraint and an important advantage compared with propeller optimisation in a fixed wake, as in e.g., Han et al (2006a), where the generated propeller thrust needs to

be considered. However, to limit the variations, it seemed reasonable to also constrain the propeller thrust to be within 10% of the initial design.

Although the above described cavitation dynamics also generate noise, the main contribution to pressure pulse nuisance comes from the pressure distribution of the loaded propeller blade moving through the water and the displacement of water by the blade thickness, including sheet cavities. These effects can be predicted with some reliability using the tools described in Section 2. Here we choose to use minimisation of the root-mean-square (rms) amplitude of the first three harmonic component (blade frequency), computed at a set of points above the shaft, as one of the objectives.

Moreover, the obvious additional objective is the efficiency of the propeller performance η, which should be maximized. To summarise this section, the sets of design variables, constraints, and objectives are listed in Table 2.

Table 2: Optimisation Parameter

Objective	η, p_{rms}
Equality constraints	V_s
Inequality constraints	CavLength/Chord, Vol_{max}/R^3, Keller
Design variables	Skew (°), Chord, Camber, Pitch

4 RESULTS

To start the optimisation, the computations are restarted from the converged baseline design. This means that first a resistance computation is carried out to develop the wake flow; a direct introduction of the propeller causes instability during the iterative update procedure. Once the flow field is developed, the propeller is introduced and the J value is adjusted to balance the propeller generated thrust with the resistance for a certain speed. Figure 8 shows the history of J and the thrust coefficient over the number of iterations. While the cavitation changes a lot in the beginning, it converges to a stable cavity prediction.

Then, for each variant the modified propeller geometry is introduced and the self-propulsion computation is restarted. At least 650 additional iterations are needed to once again achieve a converged solution. This can be observed from Figure 8, where after 4000 iterations the computation is restarted for until it converged to new J and K_T values.

4.2 Optimisation

The genetic optimisation uses 12 design variables, and is limited to 20 generations. With a population size of 12 variants, the optimisation resulted in a total of 240 computations. So, with a slightly increased mutation probability, a large design space can be investigated. For the propeller blade geometry, all these 240 variants were automatically created and computed.

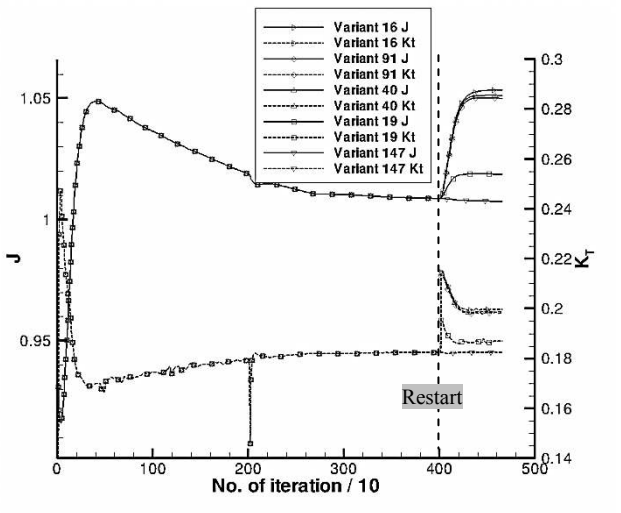

Figure 8: Convergence for J and K_T for Different Variants

While the constraint on the thrust was less strict than in the previous investigation, aiming to create more feasible design, the rotational speed was adjusted, and since the cavitation and Froude number for the cavitation prediction depends on the rotational speed in MPUF-3A, both needed to be adjusted as well. However, it appears that during the optimisation some variants result either in exceedingly loaded propellers or too high rotational speeds with the effect of implausible cavitation occurrence at various blade positions. This influenced the convergence of the optimisation algorithm in a negative way.

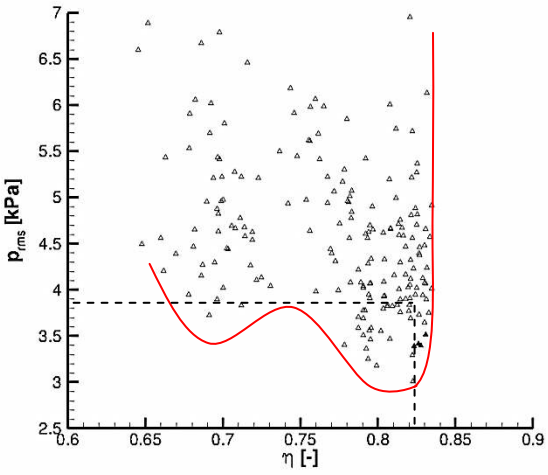

Figure 9: Pareto Front as a Result of the Optimisation Indicating the Trade-Off between Faint Efficiency Increase and Pressure Pulses

Figure 9 plots the resulting objectives for all variants, regardless if their constraints are violated or not. It shows the Pareto front of the objectives indicated by the solid line; the dashed lines indicate the position of the original design. While the range for improvement in terms of pressure pulses was significant, the efficiency showed only marginal improvement, even with increased pressure

pulses. Within a range of $\eta = 0.72$ and $\eta = 0.76$, we see a hump regarding p_{rms}. All variants in this area show violated constraints for the cavity length at the mid-section. This is also represented in the parameter value distribution of several design variables, which developed two main branches.

The best variants in comparison with the baseline design are listed in Table 3. These show a reduction of cavitation volume between 3% and up to as much as 41%. The pressure fluctuations could be reduced by up to 22% for Variant 19. However, this reduction was in conflict with the efficiency which decreased in that particular case. In fact, the optimisation algorithm had difficulties to converge to a maximum of propeller efficiency. This might be due to too strict constraints on cavitation extent.

Variants16, 91 and 40 are considered combining the best improvements in both objectives. Variant 147 shows the highest efficiency increase among the valid variants with a modest increase of 0.7%, but then with a small increase in pressure pulses.

Table 3: Optimisation Results

		V 16	V 19	V40	V 91	V 147
p_{rms}	[dB]	-0.40	-1.08	-0.53	-0.55	0.41
η	[%]	0.60	-0.40	0.05	0.25	0.71
Vol_{max}/R^3	[%]	-41.58	-3.86	-41.64	-38.83	2.77
A_E/A_0	[%]	-2.33	0.09	-1.20	-1.60	-1.23
K_T	[%]	9.41	2.40	8.91	8.77	0.0l
RPM	[%]	-4.25	-0.99	-4.04	-3.94	0.12

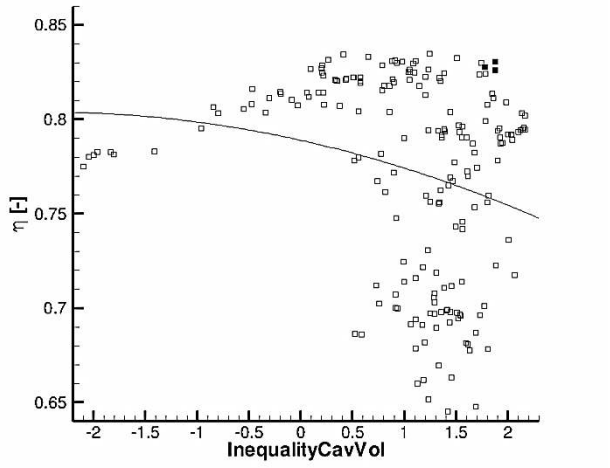

Figure 10: Efficiency Dependence on Cavity Volume

In Figure 10 the efficiency is plotted over the cavity volume constraint. A negative value means the constraint is violated with a too large cavity volume. In this figure all variants are plotted regardless if any constraints are violated or not. The black filled squares mark the best performing and not violated variants regarding both objectives (16, 40, and 91). From this figure one can see, that the most efficient variants were found with a decreased cavity volume of between 0.5 and 1.8 [Vol/R^3]. However, it shows also that even an increase of the cavity volume did not necessarily lead to an increase in efficiency.

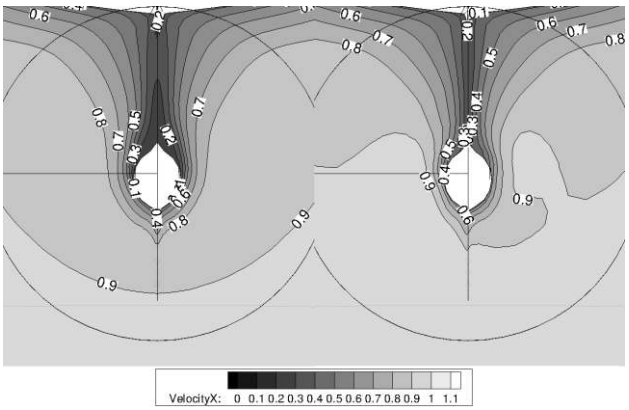

Figure 11: Axial Velocity Distribution, for the Resistance- and Self-Propelled-Computation (right)

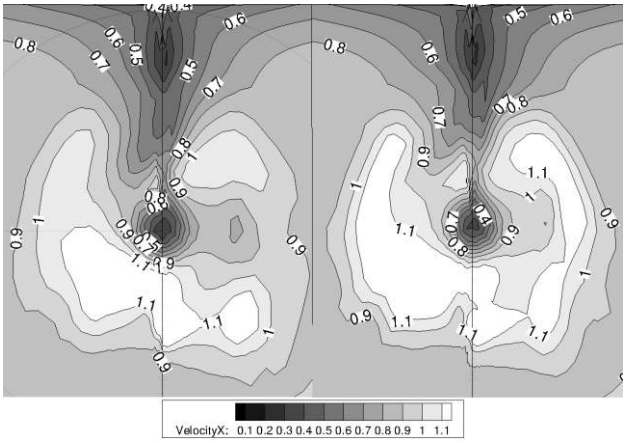

Figure 12: Axial Velocity Distribution, left for Variant 40, right for Variant 100

The effect of a propeller on the wake is shown in Figure 11 and Figure 12, where the axial velocity distribution is pictured. Figure 11 compares the flow in front of the propeller plane around the stern without and with the propeller. This comparison shows clearly how much the propeller itself affects its own inflow. A propeller experiencing the right conditions performs different than with the left inflow and certainly a propeller designed for a given flow like the left side in Figure 11, as it is commonly the case, would not perform at the optimum. Figure 12 meanwhile shows the axial velocity distribution at a plane between propeller rudder for Variant 40 and Variant 100. It shows clearly higher velocity gradients. The pressure fluctuations computed for this variant were with an increase of 2.52 dB the highest values obtained. The flow field generated from the blade design 40 is more smoothed instead. For this variant 0.53 dB less pressure fluctuations were computed, compared with the original design.

The cavitation extent for various blade angles is depicted in Figure 13. The reduction of cavity volume can be observed for all blade positions. With decreasing volume also the maximal cavitation area decreases. The effect of

this constraint on the objectives is, however, not clear, as variants with higher maximal cavitation area together may have lower induced pressure fluctuation predicted, like it is for Variant 19. This can indicate that it is the sheet thickness and its chord wise position, contributing to pressure pulses together with the variation of cavity volume, rather than the maximum.

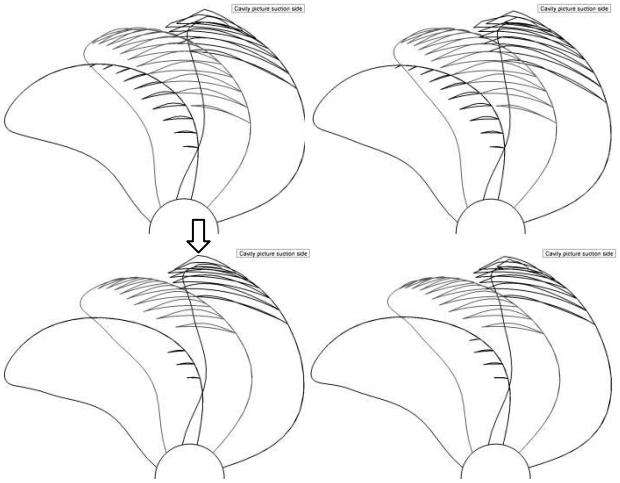

Figure 13: Cavitation Extent Baseline Design (top left), Variant with Maximum Efficiency (top right), Best Variants 16 (bottom left) and 91(bottom right)

Comparing the best Variants 16 and 91, one can see that both have similar geometry. However, while Variant 91 shows smaller pressure amplitudes, it also shows a slightly higher maximum cavity volume and area. The worse performance regarding the pressure pulses for Variant 16 might be a result of a somewhat bigger sheet thickness at the tip of Variant 16, see Figure 13.

Figure 14 to Figure 17 indicate the trends for improving the propeller blade geometry. The blade designs show only small variations for the variants from Table 3. We remark that larger geometry variations were generated during the optimisation but these violated constraints or showed worse performance.

The best performing variants regarding both objectives have a significantly increased maximum camber, except for the tip region. The effect of camber is in good agreement with Han´s optimisation in fixed wake.

This holds also for the pitch distribution. All variants perform better with a slightly higher pitch for the range between 0.4 and 0.9R, while the tip pitch is smaller than the original design. However, Variant 19 shows a remarkably higher pitch, even in the tip region, although it has the lowest pressure pulses. This might be the result of a distinctive increase of skew (less skew for smaller radii and higher skew in the tip region again) which is according to Han´s observed tendency for increased skew angels. On the other hand, the negative skew for lower radii slightly decreased and becomes positive already at radius 0.6R for the better performing variants. For larger radii, the skew angle is then much higher compared to the baseline design.

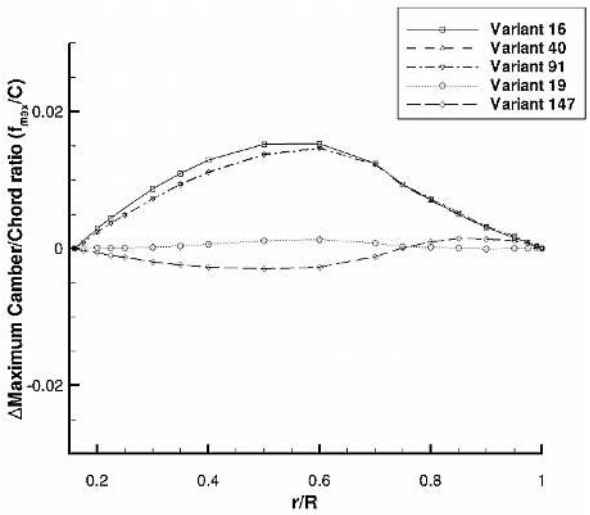

Figure 14: Maximum Camber Distribution with Respect to the Original Design along the Non-Dimensional Propeller Radius

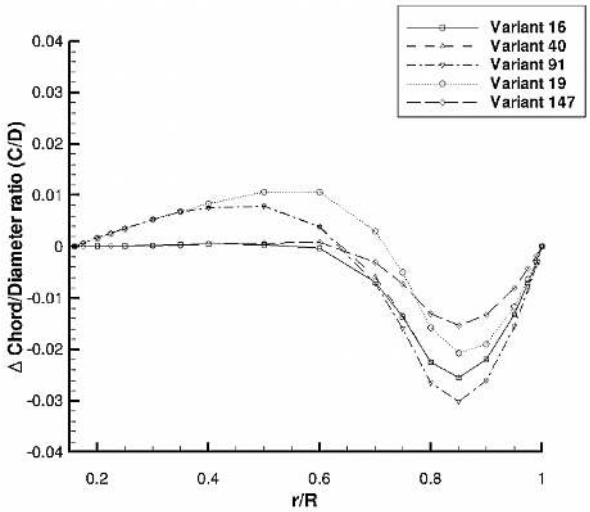

Figure 15: Chord Distribution with Respect to the Original Design along the Non-Dimensional Propeller Radius

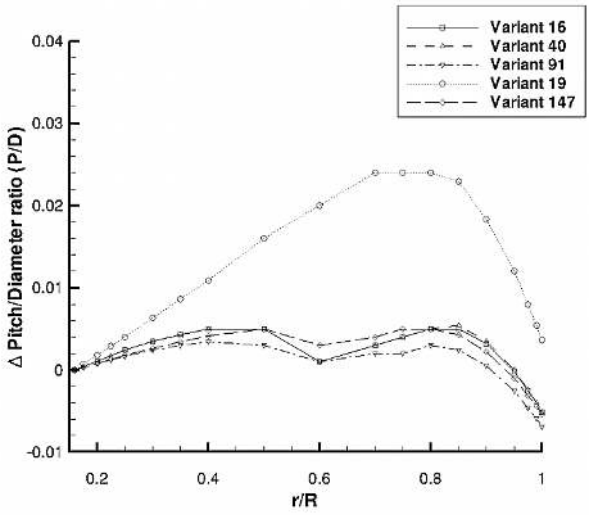

Figure 16: Pitch Distribution with Respect to the Original Design along the Non-Dimensional Propeller Radius

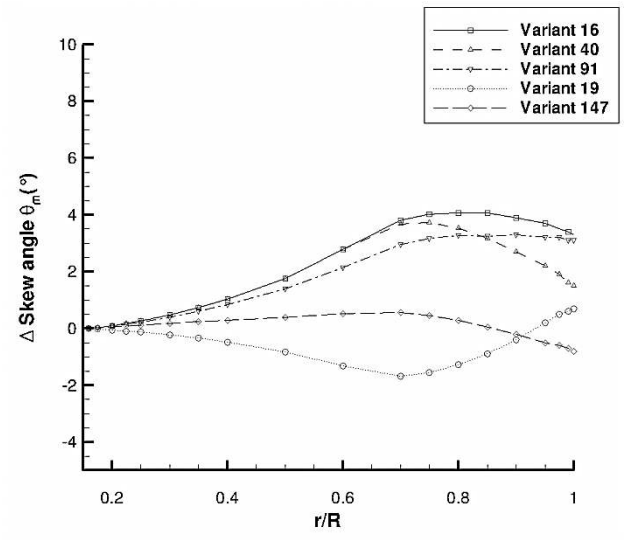

Figure 17: Skew Angle Distribution with Respect to the Original Design along the Non-Dimensional Propeller Radius

All of these variants have a smaller blade area ratio, which is again in agreement with Han´s observation. The reason is a shortened chord length distribution for the outer most radii bigger than 0.6R.

5 CONCLUSION

This investigation shows the possibility of an automated optimisation for the propeller blade design. The algorithm was able to find a better design solution regarding both of the objectives. The best design combines 8.8% smaller pressure pulses and 0.6% higher efficiency. However, it also shows that the variables, the objective functions and especially the set of constraints may be improved. The design changes should be focused on the mid-section by changing the chord, camber and pitch, while in the tip region the skew and pitch influenced the cavitation the most.

The increase of efficiency is quite small and the NSGA-II had difficulties to converge in this direction. One reason is most likely the constraints on cavitation, which were supposed to be smaller than the original design. However, none of the variants violating this constraint showed significant efficiency improvement. The variants with higher efficiency suffered almost always by higher levels of pressure pulses.

The most frequently violated constraints were the cavity length at mid-section of the blade. The maximal cavity length at the tip as well as the maximum cavity volume was rather seldom violated. However, a violation of these constraints was frequently accompanied with violated mid-section cavity length. The Keller criterion was valid for all variants but a wide range selected for the allowed K_T tolerance led to a few variants with implausible cavity occurrence.

A direct connection between the chosen constraint for cavitation volume and the pressure pulses cannot be proven. Even though almost all variants with improved pressure pulses have a lower maximal volume and the variants with improved efficiency is accompanied with an increase of cavity volume. It also occurred that variants have more cavity volume while producing less pressure pulses. This is in line with that it is actually the volume change in time having an effect in the pressure pulses.

Future work needs to be done in identifying the cavitation pattern influencing the objectives, e.g., like the tip region for Variants 16 and 91. Certain constraints may limit the possibilities to achieve better propeller performance. Furthermore, means to improve computational time, e.g., through the use of a response surface or space mapping techniques, should be investigated.

ACKNOWLEDGEMENT

This work has been carried out within the Rolls-Royce UTC in Computational Hydrodynamics at Chalmers, with the support from the Hydrodynamic Research Centre of Rolls-Royce AB, FRIENDSHIP-SYSTEMS and Flowtech International AB.

REFERENCES

Abraham, A., Jain, L. & Goldberg, R. (2005). Evolutionary Multiobjective Optimization. Springer Verlag.

Abt, C., Harries, S. & Wunderlich, S. (2009). 'Flexible Tool Integration for Simulation-driven Design using XML, generic and COM Interfaces'. 8th International Conference on Computer Applications and Information Technology in Maritime Industries (COMPIT), Hungary, Budapest.

Bark, G., Berchiche, N. & Grekula, M. (2004). Application of principles for the observation and analysis of eroding cavitation – The EROCAV observation handbook. Department of Naval Architecture and Ocean Engineering, Chalmers University of Technology.

Bertram, V. (2000). Practical Ship Hydrodynamics. Butterworth-Heinemann.

Branke, J., Deb, K., Miettinen, K. & Slowinski, R. (2008). Multiobjective Optimization. Springer Verlag.

Carlton, J. (2007). Marine propellers and propulsion. Butterworth-Heinemann.

Deb, K., Agrawal, S., Pratap, A. & Meyarivan, T. (2000). 'A Fast Elitist Non-dominated Sorting Genetic Algorithm for Multi-objective Optimization: NSGA-II'. Proceedings of the 6th International Conference on Parallel Problem Solving from Nature.

Foeth, E.-J. (2008). The structure of three-dimensional sheet cavitation. PhD Thesis, Delft University.

Grekula, M. (2010). Cavitation Mechanisms Related to Erosion. PhD Thesis, Chalmers University of Technology.

Han, K.-J., Bark, G, Larsson, L. & Regnström, B. (2006). 'A Procedure for Optimizing Cavitating Propeller Blades'. Ship Technology Research **53**.

Han, K.-J., Larsson, L. & Regnström, B. (2006). 'Numerical optimization of the propeller behind aa ship hull at full scale'. 26th Symposium on Naval Hydrodynamics, Rome, Italy.

Han, K.-J., Larsson, L. & Regnström, B. (2008). 'A numerical study on hull/propeller/rudder interaction'. 27th Symposium on Naval Hydrodynamics, Seoul, Korea.

He, L., Chang, S. & Kinnas, S. (2010). 'MPUF-3A Version 3.0'. User's manual and documentation. University of Texas.

Kerwin, J. & Kinnas, S. (1986). 'Experimental and Analytical Techniques for the Study of Unsteady Propeller Sheet Cavitation'. 16th Symposium on Naval Hydrodynamics, Berkley, California.

Kim, K. & Li, Da-qing. (2010). 'Estimation of Numerical Uncertainty of SHIPFLOW 4.4 in Self-propulsion Simulation of KCS'. Gothenburg 2010 Workshop on Numerical Ship Hydrodynamics **2**, pp. 423-428.

Kim, J., Park,I.-R., Kim, K.-S. & Van, S.-H. (2010). 'Feasibility study on numerical towing tank application to predictions of resistance and self-propulsion performance for a ship'. Gothenburg 2010 Workshop on Numerical Ship Hydrodynamics **2**, pp. 563-568.

Kinnas, S. (1985). Non-linear correction to the linear theory for the prediction of the cavitating flow around hydrofoils. PhD Thesis, Massachusetts Institute of Technology.

Kinnas, S. & Young, Y. L. (2003). 'Modelling of cavitating or ventilated flows using BEM'. International Journal of Numerical Methods for Heat & Fluid Flow **13**(6), pp. 672-694.

Kinnas, S. & Hsin, C.-Y. (1994)**.** 'The local error of a low-order Boundary element Method at the trailing edge of a hydrofoil and its effect on the global solution'. Computers and Fluids **23**(1) pp. 63-75.

Kinnas, S., HanSeong, L. & Young, Y.L. (2003). 'Modeling of Unsteady Sheet Cavitation on Marine Propeller Blades'. International Journal of Rotating Machinery **9**, pp. 263-277.

Kinnas, S., Hon, S. & HanSeong, L. (2003). 'Numerical Analysis of Flow Around the Cavitating Hydrofoil'. 5th International Symposium on Cavitation, Osaka, Japan.

Kupier, G. (2010). 'New development and propeller design'. 9th International Conference on Hydrodynamics, Shanghai, China.

Lee, S.-K., Liao, M. & Wang, S. (2006). 'Propeller-Induced Hull Vibration – Analytical Methods'. Proceedings of the 2nd International Ship Noise and Vibration Conference, London, UK.

Mishima, S. (1996). Design of Cavitating Propeller Blades in Non-Uniform Flow by Numerical Optimization. PhD Thesis, Massachusetts Institute of Technology Department of Ocean Engineering.

Sirinivas, N. & Deb, K. (1995). 'Multi-Objective function optimization using non-dominated sorting genetic algorithms'. Evolutionary Computation **2**, pp. 221-248.

Sun, H. & Kinnas, S. (2007). 'HULLFPP, HULL Field Point Potential'. User's manual and documentation. University of Texas.

Regnström, B. (2007). XCHAP theoretical manual. Flowtech International AB.

Visonneau M. (2010). 'Analysis of G2010 results for test cases 1.1a, 2.1, 2.3a, 3.1a, 3.1b, 3.5 and 3.6 Local flow analysis'. Gothenburg 2010 Workshop on Numerical Ship Hydrodynamics **1**.

Zou, L, & Larsson, L. (2010). 'CFD prediction of the local flow around the KVLCC2 tanker in fixed conditions'. Gothenburg 2010 Workshop on Numerical Ship Hydrodynamics **2**, pp. 423-428.